

ORIGINAL ARTICLE

Open Access



# GNSS gyroscopes: determination of angular velocity and acceleration with very high-rate GNSS

Yun Shi<sup>1</sup>, Peiliang Xu<sup>2\*</sup> , Yuanming Shu<sup>3</sup> and Xiaolin Meng<sup>4</sup>

## Abstract

Although global navigation satellite systems (GNSS) have been routinely applied to determine attitudes, there exists no literature on determining angular velocity and/or angular acceleration from GNSS. Motivated by the invention of computerized accelerometers of the correspondence author and following the success of accurately recovering translational velocity and acceleration waveforms from very high-rate GNSS precise positioning by Xu and his collaborators in 2021, we propose the concept of GNSS gyroscopes and reconstruct angular velocity and acceleration from very high-rate GNSS attitudes by applying regularization under the criterion of minimum mean squared errors. The major results from the experiments can be summarized in the following: (i) angular velocity and acceleration waveforms computed by applying the difference methods to high-rate GNSS attitudes are too noisy and can be physically not meaningful and numerically incorrect. The same can be said about inertial measurement unit (IMU) attitudes, if IMU gyros are not of very high accuracy; (ii) regularization is successfully applied to reconstruct the high-rate angular velocity and acceleration waveforms from 50 Hz GNSS attitudes and significantly outperforms the difference methods, validating the proposed concept of GNSS gyroscopes. By comparing the angular velocity and acceleration results by using the difference methods and regularization, we find that the peak values of angular velocity and acceleration by regularization are much smaller by a maximum factor of 1.57 in the angular velocity to a maximum factor of 8662.53 times in the angular acceleration in the case of high-rate GNSS, and by a maximum factor of 1.26 in the angular velocity to a maximum factor of 2819.85 times in the angular acceleration in the case of IMU, respectively; and (iii) the IMU attitudes apparently lead to better regularized angular velocity and acceleration waveforms than the high-rate GNSS attitudes, which can well be explained by the fact that the former is of better accuracy than the latter. As a result, to suppress the significant amplification of noise in GNSS attitudes, larger regularization parameters have to be chosen for the high-rate GNSS attitudes, resulting in smaller peak angular accelerations by a maximum factor of 37.55 percent in the angular velocity to a maximum factor of 6.20 times in the angular acceleration in comparison of the corresponding IMU results. Nevertheless, the regularized angular acceleration waveforms for both GNSS and IMU look more or less similar in pattern or waveform shape.

**Keywords** Angular velocity, Angular acceleration, High-rate GNSS, GNSS attitudes, GNSS gyroscopes, Regularization

\*Correspondence:

Peiliang Xu

pxu@rcep.dpri.kyoto-u.ac.jp

Full list of author information is available at the end of the article



© The Author(s) 2024. **Open Access** This article is licensed under a Creative Commons Attribution 4.0 International License, which permits use, sharing, adaptation, distribution and reproduction in any medium or format, as long as you give appropriate credit to the original author(s) and the source, provide a link to the Creative Commons licence, and indicate if changes were made. The images or other third party material in this article are included in the article's Creative Commons licence, unless indicated otherwise in a credit line to the material. If material is not included in the article's Creative Commons licence and your intended use is not permitted by statutory regulation or exceeds the permitted use, you will need to obtain permission directly from the copyright holder. To view a copy of this licence, visit <http://creativecommons.org/licenses/by/4.0/>.

## Introduction

Attitude information represents the three-dimensional (3D) orientation of an object or body relative to a reference frame, e.g., the East-North-Up/Down system, at a certain time, plays an increasingly more important role and finds many applications in different areas of science and engineering. In positioning, navigation, mapping, guidance and control, attitude is used to connect the motion of an object such as spacecraft, vehicles, ships and unmanned vehicles in the air or under water at different time epochs (see e.g., Cohen 1992; Cohen et al., 1993; Eling et al. 2015; Lachapelle et al., 1996; Lu 1995; Lu et al., 1994; Kinsey et al., 2006; Shu et al., 2022; Xu et al., 2019). It is also essential for spacecraft rendezvous and docking (see e.g., Bashnick & Ulrich 2023; Segal et al. 2014; Zhao & Zhang 2022). In geophysics and seismology, although rotational motion due to earthquakes is small (Reid 1910), precise modern attitude technology makes it possible to measure a small rotation, which leads to a new research direction for seismology, namely, rotational seismology (see e.g., Igel et al., 2007; Lee et al., 2009; Takeo 2009). Global navigation satellite systems (GNSS) can also become a potential technology to contribute to rotational seismology (Xu et al., 2019). Mobile robot location and autonomous navigation could not be possible without attitude either (see e.g., Hashim & Lewis 2021; Islam et al., 2019; Royer et al., 2007). With more cameras installed in public areas, attitude has been shown to be essential in pose determination and tracking of human beings and moving objects (see e.g., De Vito et al., 2016; Fujiwara & Yokomitsu 2021; Linnainmaa et al., 1988; Richards 1999), detecting dangerous objects (Fujii et al., 2020), playing a key role in medical health care and rehabilitation (De Vito et al., 2014; Endo et al., 2023), predicting children's behavior to prevent fall accidents (Nose et al., 2020), and even recognizing the smoking poses of people (Jeong & Ha 2023).

Attitude can be directly measured with physical instruments. Gyroscopes have been well known to directly measure the attitude or angular rotation of a body, since Foucault invented gyroscopes to demonstrate the Earth's rotation in 1852 (see e.g., Bertrand 1857; Bennett 1970; Sommeria 2017; Passaro et al., 2017; Tobin 2023), though its play origin was reported to be with the Chinese spinning top. They can basically be classified into three different classes: mechanical, optical and vibratory, because they are designed and fabricated with different principles of physics and technology (see e.g., Armenise et al., 2010; Cordeiro 1913; Passaro et al., 2017; Yazdi et al., 1998). The first two classes of gyroscopes essentially measure angular rotations, while the third class is to reconstruct angular rates through sensing physical effects. More precisely, conventional gyroscopes are all mechanical

and work after the physical principle of conservation of angular momentum that a rigid body rotating or spinning at a high speed around an axis maintains its orientation with respect to an inertial space. They have successfully been applied in airplane, spacecraft and satellite navigation. Nevertheless, mechanical gyroscopes are difficult to miniaturize and a slight external force will substantially change the plane of rotation after a sufficiently long time (Cordeiro 1913). The second class of gyroscopes are optical, which operates on the physical basis of Sagnac effect. If a light wave is split into two beams travelling along a rotating ring in opposite directions, Sagnac effect states that the time difference between the two light beams finishing their travels in the ring is proportional to the angular rotation of the ring. As a result, Sagnac effect has been widely implemented to design and fabricate optical gyroscopes such as Ring Laser Gyros and Fiber-optic gyroscopes. Major problems with optical gyroscopes include: (i) null shift in the case of zero angular rate, which is not predictable and time-varying; (ii) scale factor, which may not be equal to its nominal value; and (iii) if the angular rate is below a critical value, the two beams of light are locked and no measurement of Sagnac effect is possible. The third class of gyroscopes are vibratory gyros, which use Coriolis effect to measure rotational rates. Because vibratory gyros do not require a large ring nor a spinning mass and can be technologically miniaturized, all microelectromechanical system (MEMS) gyroscopes belong to this class. For more details, the reader is referred to, for example, Armenise et al. (2010).

Attitude can also be indirectly determined from measurements such as GNSS and video images. The basic idea of all indirect methods to determine the attitudes of a rigid body in the 3D space is to first select three non-collinear points on the body, determine their 3D coordinates and then use them to compute the rotational angles of the body (or equivalently, the orientation of the plane defined by the three points) with respect to a certain reference frame. General mathematical methods to analytically or numerically determine attitudes can be found, for example, in Schönemann (1964), Wahba (1965), Keat (1977), Horn et al. (1988) and Crassidis et al. (2007). To determine the attitudes of a vehicle from GNSS, one can first install three GNSS antennas, dedicated or non-dedicated, on the vehicle, use GNSS observables to determine the 3D positions of the antennas and finally compute the attitudes of the vehicle. Depending on different objects of interest, the types of GNSS observables and the (absolute or relative) methods to solve for the positions of GNSS antennas, different methods of GNSS attitude determination have been proposed and widely applied in manned and unmanned navigation (see e.g., Cannon & Sun 1996; Cohen 1992; Cohen et al., 1993; Evans 1986; Eling et al.,

2015; Lachapelle et al., 1996; Lu 1995; Lu et al., 1994; Kinsey et al., 2006; Shu et al., 2022) and rotational seismology (Xu et al., 2019). In a similar manner, if a vehicle or a robot is captured simultaneously by at least two video cameras with known positions, one can then determine the attitudes of the vehicle/robot (see e.g., Royer et al. 2007; Islam et al., 2019; Hashim & Lewis 2021). The same idea applies to determining the pose of a person as well (see e.g., Endo et al., 2023; Fujiwara & Yokomitsu 2021; De Vito et al., 2016; Fujii et al., 2020; Linnainmaa et al., 1988; Nose et al., 2020; Richards 1999).

Although attitudes can either be directly measured or indirectly determined, we can only compute angular velocity or acceleration with them, which is, unfortunately, well known as an inverse ill-posed problem (Xu 2023; Xu et al., 2021). It is interesting to note that treating the reconstruction of accelerations from noisy measurements as an inverse ill-posed problem directly leads to the invention of computerized accelerometers (Xu 2023). In other words, if we apply the conventional weighted least squares (LS) or difference methods to compute velocities and/or accelerations from positions or displacements, the results will be too noisy to be physically useful or meaningful and even numerically incorrect. As basic physical quantities, angular velocity and acceleration are of the same fundamental importance as translational velocity and acceleration in science and engineering. For example, vehicle safety and control require precise knowledge of the yaw rate (see e.g., Chindamo et al., 2018; Leung et al., 2011; Xia et al., 2023). Thus, the main purpose of this paper is to propose the concept of GNSS gyroscopes.

Since GNSS attitude determination has been well addressed in the literature, we will focus on the determination of angular velocity and acceleration from high-rate GNSS in this paper, which describe the changes in angular position and angular velocity per unit time, respectively. From this point of view, we may say that this work is a direct extension of Xu et al. (2021) and Xu (2023) to angular velocity and acceleration. More precisely, we will follow Xu et al. (2021) to present regularization for the determination of angular velocity and acceleration with high-rate GNSS attitudes in Section 2. Section 3 will briefly outline our high-rate GNSS attitude experiments conducted almost ten years ago and use the experimental results to further determine angular velocity and acceleration. Section 4 reports the experimental results of angular velocity and acceleration by applying the difference methods to high-rate GNSS and IMU attitudes. In Sections 5 and 6, we will focus on the regularized solutions of angular velocity and acceleration and their comparisons obtained with both GNSS and IMU measurements, respectively.

## Regularized solutions of angular velocity and acceleration with high-rate GNSS attitudes

### High-rate GNSS attitude determination

In this work, we follow a two-step approach to determine high-rate GNSS attitudes, namely, first solve the baselines between each pair of antennas and then use them to determine the attitudes. If the reader is interested in one step approach, namely to determine attitude directly from raw GNSS observables, he or she may refer to Cohen (1992) and Lu (1995), for example. Although both PPP and relative positioning modes can be used to determine a baseline, we use the latter mode for our purpose. It can result in a more precise baseline solution for a short baseline, because almost all systematic errors could be theoretically cancelled out through double difference (see e.g., Hofmann-Wellenhof et al., 1992). Indeed, the relative positioning mode has been shown to perform better than PPP mode for GNSS attitude determination (Shu et al., 2022; Xu et al., 2019).

In the case of multi-GNSS constellations and based on the relative positioning mode, one may solve for the precise baselines either with each GNSS constellation or by combining all the constellations to obtain the optimal combined multi-GNSS baseline solutions. For simplicity, let us assume three antennas and we can obtain a number of baseline solutions from multi-GNSS constellations, which are given in the local level NED frame and denoted by  $(\mathbf{u}_1^{g_i}, \mathbf{u}_2^{g_i})$ , where the superscript  $g_i$  stands for the  $i$ th GNSS constellation or the multi-GNSS constellation. In a similar manner, let us denote the baseline vectors of antennas in the body frame by  $(\mathbf{b}_1, \mathbf{b}_2)$ . We can then connect the baseline vectors in the body frame to the observed baselines through the unknown attitude matrix  $\mathbf{R}$ . If  $\mathbf{R}$  is represented by using the three Euler angles, then it automatically satisfies the conditions, namely,  $\mathbf{R}^T \mathbf{R} = \mathbf{R} \mathbf{R}^T = \mathbf{I}_3$  and  $\det\{\mathbf{R}\} = 1$ , where  $\det\{\mathbf{R}\}$  stands for the determinant of  $\mathbf{R}$  and  $\mathbf{I}_3$  is a  $(3 \times 3)$  identity matrix. Before we can apply the weighted LS method to determine the unknown attitude rotation matrix  $\mathbf{R}$ , we assume the weight matrix for both  $\mathbf{u}_1^{g_i}$  and  $\mathbf{u}_2^{g_i}$  and denote it by  $\mathbf{W}_{g_i}$ . Collecting the baseline solutions from all the multi-GNSS constellations, we can then apply the following weighted LS objective function:

$$\min : \sum_{j=g_1}^{g_m} \begin{bmatrix} \mathbf{u}_1^j - \mathbf{R}\mathbf{b}_1 \\ \mathbf{u}_2^j - \mathbf{R}\mathbf{b}_2 \end{bmatrix}^T \mathbf{W}_j \begin{bmatrix} \mathbf{u}_1^j - \mathbf{R}\mathbf{b}_1 \\ \mathbf{u}_2^j - \mathbf{R}\mathbf{b}_2 \end{bmatrix}, \quad (1)$$

to solve for the attitude matrix  $\mathbf{R}$ .

If the correlations between  $\mathbf{u}_1^j$  and  $\mathbf{u}_2^j$  are negligibly small, the minimization problem (1) becomes

$$\min : \sum_{j=g_1}^{g_m} \{(\mathbf{u}_1^j - \mathbf{Rb}_1)^T \mathbf{W}_{1j} (\mathbf{u}_1^j - \mathbf{Rb}_1) + (\mathbf{u}_2^j - \mathbf{Rb}_2)^T \mathbf{W}_{2j} (\mathbf{u}_2^j - \mathbf{Rb}_2)\}, \quad (2)$$

where  $\mathbf{W}_{1j}$  and  $\mathbf{W}_{2j}$  are the weight matrices of the baseline solutions  $\mathbf{u}_1^j$  and  $\mathbf{u}_2^j$ , respectively. In particular, if  $\mathbf{W}_{1j} = w_{1j} \mathbf{I}_3$  and  $\mathbf{W}_{2j} = w_{2j} \mathbf{I}_3$ , the above objective function (2) is further simplified as

$$\min : \sum_{j=g_1}^{g_m} \{w_{1j} (\mathbf{u}_1^j - \mathbf{Rb}_1)^T (\mathbf{u}_1^j - \mathbf{Rb}_1) + w_{2j} (\mathbf{u}_2^j - \mathbf{Rb}_2)^T (\mathbf{u}_2^j - \mathbf{Rb}_2)\}, \quad (3)$$

which is the estimation criterion to determine the attitudes first proposed by Wahba (1965). If a GNSS constellation can only provide a baseline, say only  $\mathbf{u}_1^j$ , then  $\mathbf{W}_{2j} = \mathbf{0}$  or equivalently,  $w_{2j} = 0$ . Based on the idea of Davenport, Keat (1977) published a technical report to analytically solve for the rotation matrix  $\mathbf{R}$  in (3) and further to compute the three Euler angles. For more technical details and other attitude solution methods, the reader may refer to Keat (1977), Horn et al. (1988), Black (1964), Markley (2002), Shuster & Oh (1981), Markley & Mortari (2000), Crassidis et al. (2007) and Xu et al. (2019).

### Regularized solutions of angular velocity and acceleration functions

In principle, the starting differential equations to reconstruct angular velocity and acceleration from high-rate GNSS are essentially the same as those to reconstruct (translational) velocity and acceleration. The only difference is that observations for the former are high-rate GNSS attitudes, while those for the latter are high-rate GNSS positions or displacements. Thus, following Xu et al. (2021) and Xu (2023), we can readily write the differential equations for angular velocity as follows:

$$\frac{d\theta(t)}{dt} = \omega(t), \quad (4)$$

where  $\theta(t)$  is the GNSS-determined angular position/attitude of a rigid body at the time  $t$  and  $\omega(t)$  is the angular velocity of the body at the time  $t$ . As the first aspect of GNSS gyroscopes in this paper, we will determine the angular velocity function  $\omega(t)$  from the GNSS angular function  $\theta(t)$ . Following Xu et al. (2021), we will have to first rewrite the differential equation (4) as the following Volterra's integral equation of the first kind:

$$\theta(t) = \int_{t_0}^t \omega(\tau) d\tau + \theta(t_0). \quad (5)$$

In practice, it is not possible for us to obtain the continuous GNSS angular function  $\theta(t)$  over a time interval  $[0, t]$ . Instead, we can only determine  $\theta(t)$  at the discrete time instants  $(t_0, t_1, t_2, \dots, t_n)$  and accordingly reconstruct the GNSS angular velocity function  $\omega(t)$  at the discrete time instants.

In a similar manner, we can write the differential equations for angular acceleration as follows:

$$\frac{d^2\theta(t)}{dt^2} = \alpha(t), \quad (6)$$

or equivalently, in the form of Volterra's integral equation of the first kind:

$$\theta(t) = \int_{t_0}^t (t - \tau) \alpha(\tau) d\tau + (t - t_0) \omega(t_0) + \theta(t_0), \quad (7)$$

(see e.g., Lonseth 1977; Lubansky et al., 2006; Xu 2023; Xu et al., 2021), where  $t_0$  and  $\theta(t_0)$  have been defined in (5),  $\alpha(t)$  is the angular acceleration function to be estimated from the angular position function  $\theta(t)$ ,  $\omega(t_0)$  is the angular velocity at the time instant  $t_0$ . As in the case of GNSS angular velocity, given the angular positions/attitudes  $\theta(t)$  at the discrete time instants  $(t_0, t_1, t_2, \dots, t_n)$ , our purpose is to reconstruct the GNSS angular acceleration function  $\alpha(t)$  at the discrete time instants.

To determine the angular velocity  $\omega(t)$  and/or acceleration  $\alpha(t)$  from the GNSS angular position  $\theta(t)$ , and bearing in mind that  $\theta(t)$  has only been sampled at discrete time epochs, we have to discretize the integral equations (5) and (7) by applying a certain rule of numerical integration. We may note that different rules of numerical integration can be applied to discretize (5) and (7), respectively. In this paper, we follow Xu et al. (2021) (see also Xu 2023) and choose the Trapezoidal rule for both (5) and (7). As a result, we obtain the following linearized observation equation:

$$\mathbf{y} = \mathbf{A}\boldsymbol{\beta} + \boldsymbol{\epsilon}, \quad (8)$$

where the observations  $\mathbf{y}$  of GNSS angular positions are given by  $\mathbf{y} = [\theta(t_0), \theta(t_1), \theta(t_2), \dots, \theta(t_n)]^T$ ,  $\theta(t_i)$  can represent one of the GNSS attitude angles, namely, yaw, pitch or roll at the time epoch  $t_i$ ,  $\boldsymbol{\beta}$  stands for the discrete values of either angular velocity  $\omega(t)$  in the case of (5) or angular acceleration  $\alpha(t)$  in the case of (7). If the initial parameter  $\theta(t_0)$  or  $\omega(t_0)$  or both are unknown, they should be included into  $\boldsymbol{\beta}$ .  $\mathbf{A}$  is the coefficient matrix, and  $\boldsymbol{\epsilon}$  is the random error vector of the GNSS angular measurements  $\mathbf{y}$ . The GNSS angular position error vector  $\boldsymbol{\epsilon}$

is assumed to be of mean zero and variance-covariance matrix  $\mathbf{W}^{-1}\sigma^2$ , where  $\mathbf{W}$  is the weight matrix and  $\sigma^2$  the (given or unknown) variance of unit weight.

Because the Volterra's integral equations (5) and (7) are of the first kind, they are ill-posed. As a result, the discretized observation equation (8), either to reconstruct the angular velocities or the angular accelerations from high-rate GNSS angular positions, must be ill-conditioned. With the increase of the reconstruction resolution, the condition number of the coefficient matrix  $\mathbf{A}$  can be very large such that the naive weighted LS estimate of  $\boldsymbol{\beta}$  can be too noisy to be physically useful or meaningful. Thus, we have to apply regularization to (8) in order to obtain a stable and accurate solution of  $\boldsymbol{\beta}$ . There exist a number of regularization methods to stably and accurately reconstruct the angular velocity and acceleration, for example, ridge regression and regularization (Phillips 1962; Hoerl & Kennard 1970; Tikhonov & Arsenin 1977; Xu 1992), Bayesian inference criterion (Akaike 1980; Tarantola 1987; Xu 2021), generalized cross-validation (Golub et al., 1979; Xu 2009) and truncation of singular value decomposition (Xu 1998). In this work, we will follow Xu (1992, 2023) and Xu et al. (2021) and use the criterion of minimum mean squared error to estimate the angular velocities and/or angular accelerations  $\boldsymbol{\beta}$ . More precisely, given a value of the (positive) regularization parameter  $\kappa$ , we will minimize the following objective function:

$$\min: F(\boldsymbol{\beta}) = (\mathbf{y} - \mathbf{A}\boldsymbol{\beta})^T \mathbf{W}(\mathbf{y} - \mathbf{A}\boldsymbol{\beta}) + \kappa \boldsymbol{\beta}^T \mathbf{S} \boldsymbol{\beta}, \quad (9)$$

to estimate the unknown angular velocities and/or angular accelerations. The matrix  $\mathbf{S}$  is formulated or required to satisfy the smoothness of the second derivatives of the angular velocity or acceleration function (see e.g., Phillips 1962). Since it is generally not of full rank, we further follow Xu et al. (2021) by adding the identity matrix to obtain the final smoothness matrix, which, without confusion, is still denoted by  $\mathbf{S}$ . As a result, we can finally obtain the regularized solution of  $\boldsymbol{\beta}$ , denoted by  $\hat{\boldsymbol{\beta}}_\kappa$ , as follows:

$$\hat{\boldsymbol{\beta}}_\kappa = (\mathbf{A}^T \mathbf{W} \mathbf{A} + \kappa \mathbf{S})^{-1} \mathbf{A}^T \mathbf{W} \mathbf{y}, \quad (10)$$

where  $\kappa$  is the regularization parameter, which is determined by applying the criterion of minimum mean squared errors (MSE) after Xu et al. (2021) and Xu (2023). The bias of  $\hat{\boldsymbol{\beta}}_\kappa$  in (10) is denoted by  $\text{bias}(\hat{\boldsymbol{\beta}}_\kappa)$  and simply given below:

$$\text{bias}(\hat{\boldsymbol{\beta}}_\kappa) = -\kappa (\mathbf{A}^T \mathbf{W} \mathbf{A} + \kappa \mathbf{S})^{-1} \mathbf{S} \boldsymbol{\beta}. \quad (11)$$

By substituting  $\boldsymbol{\beta}$  with its regularized solution  $\hat{\boldsymbol{\beta}}_\kappa$ , we may estimate  $\text{bias}(\hat{\boldsymbol{\beta}}_\kappa)$ . However, we should note that such an estimate is also biased because  $\hat{\boldsymbol{\beta}}_\kappa$  is biased and its accuracy depends on that of  $\hat{\boldsymbol{\beta}}_\kappa$ .

## Experimental setups for high-rate GNSS gyroscopes

As part of our effort to investigate high-rate GNSS attitude determination in the past ten years or so, we installed three Trimble Net R9 antennas on a GNSS experimental platform on the roof of a 16-story building (the tallest buildings in its surrounding), where the Wuhan University GNSS Research Center was located. The first sets of experiments were performed on March 22 and August 22, 2014, respectively. The experimental results of high-rate GNSS attitude determination were reported in Xu et al. (2019), which were further extended to determine vehicular attitudes (Shu et al., 2022). It is interesting to note that these experiments fit the purposes of demonstrating the theory and methods in the current work well, namely, (i) to demonstrate the determination of angular velocity and acceleration from high-rate GNSS attitudes, and (ii) to compare the GNSS high-rate angular velocity and acceleration with the results from the optical gyros. The raw data of angular rates from the optical gyros of the installed IMU was not used in the research of GNSS attitude determination mentioned above but becomes now scientifically very valuable to compare high-rate GNSS angular velocity and acceleration in the current study. To give the reader a rough idea about our experiments, we show the experimental platform in Fig. 1. The reader is referred to Xu et al. (2019) for more information.

The experiments of high-rate GNSS attitude determination on March 22 and August 22, 2014 were involved with multi-constellations, namely, GPS, BeiDou, GLO-NASS and Galileo. The individual and combined multi-constellation high-rate GNSS attitudes were determined, both in relative positioning mode and PPP mode, analyzed and reported in Xu et al. (2019). In this section, we will limit ourselves to the combined multi-constellation high-rate GNSS attitude determination in relative positioning mode and simply just use the attitude results on August 22, 2014 to demonstrate the new theory and method proposed in this paper. Since the raw IMU attitudes are very important for this research, it is appropriate to show the GNSS-determined attitudes in the IMU frame for the purpose of comparison.

Although the combined multi-constellation high-rate GNSS attitude results on the right hand sides of Fig. 8 of Xu et al. (2019) last for about 250 seconds, we should note that there exist a few seconds of data gaps. Thus, to give the reader a clear impression of GNSS and IMU attitudes, we focus on the beginning parts of about 106 seconds combined multi-constellation high-rate GNSS attitude results there without any data gap, which are reproduced in Fig. 2 under the IMU frame and will be used to demonstrate the concept of GNSS gyroscopes

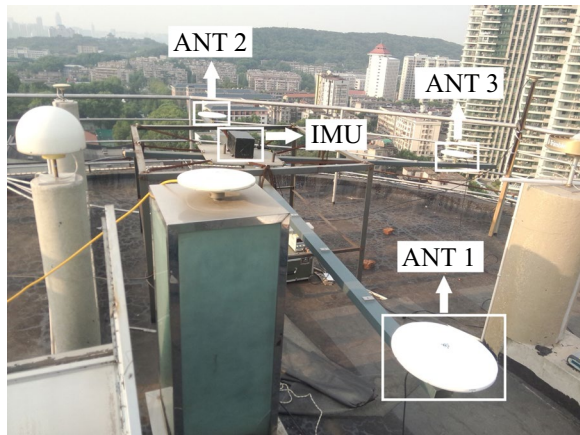


**Fig. 1** The experimental platform of high-rate GNSS gyroscopes with the three Trimble Net R9 antennas and the inertial measurement unit IMU-NV-LINS812

in this paper. Because the IMU attitudes in Fig. 8 of Xu et al. (2019) were GNSS-aided, we decide not to use them here. Instead, we will only limit ourselves to the raw IMU attitudes obtained purely from the optical gyros of the installed IMU NV-LINS812 without GNSS aid. The IMU was made by NAV Technology Co. Ltd., China, and reported to be of the accuracy of 0.003, 0.003 and 0.005 degree (or deg in the remainder of this paper) for roll, pitch and yaw, respectively, if aided with GNSS. The raw IMU attitudes from the optical gyros, corresponding to the continuous GNSS attitude solutions, are shown in panel B on the right hand side of Fig. 2. For this study,

we use the first 18 s of the static GNSS and IMU attitudes to estimate the standard deviations of these data, which are equal to 0.0628, 0.0379 and 0.0183 deg in roll, pitch and yaw in the case of GNSS, and 0.0056, 0.0019 and 0.0033 deg in roll, pitch and yaw in the case of IMU, respectively. The standard deviations of IMU attitudes are roughly consistent with the reported accuracy by the maker, though the latter are reported to be GNSS-aided. The IMU attitudes are much more precise than the GNSS ones by a factor of 4.55 to 18.95.

To further understand the high-rate GNSS and IMU attitudes, we use the first 18 s of static GNSS and IMU attitudes and compute the serial correlation coefficients for each component of attitudes, whose correlograms are shown in Fig. 3. The GNSS attitudes show a strong correlation within a short time of 0.04 s, with the first two serial correlation coefficients being equal to 0.7994 and 0.4833 in roll, 0.7836 and 0.4712 in pitch, and 0.8383 and 0.5528 in yaw. The serial correlation coefficients with a time lag of 0.06 s and beyond are apparently very small, implying that the GNSS attitudes can be treated as almost uncorrelated after three epochs. On the other hand, it is surprised to see from panel B of Fig. 3 that the serial correlation coefficients of the 200 Hz IMU static attitudes remain high above 0.9 and even almost 0.996 after 300 epochs (or equivalently 1.5 s) in yaw and roll, respectively. All the three series of correlation coefficients exhibit anomalous periodic variations for roll, pitch and yaw. If we down-sample from 200 Hz to 50 Hz, then the serial correlation coefficients remain above 0.5 up to 0.26 s in yaw and 2.26 s in pitch. These values remain above 0.5 up

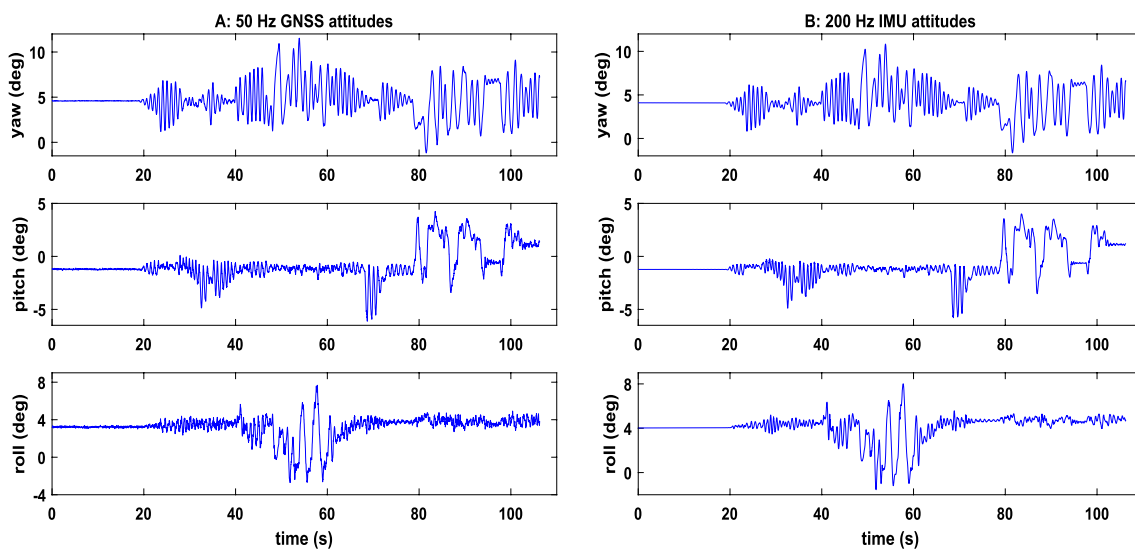


**Fig. 2** The combined multi-constellation 50 Hz GNSS attitudes in the IMU frame and the 200 Hz IMU raw attitudes from the optical gyros of the installed IMU NV-LINS812. Panel A on the left side shows the GNSS attitudes, while panel B on the right side plots the raw attitudes from the gyros of NV-LINS812

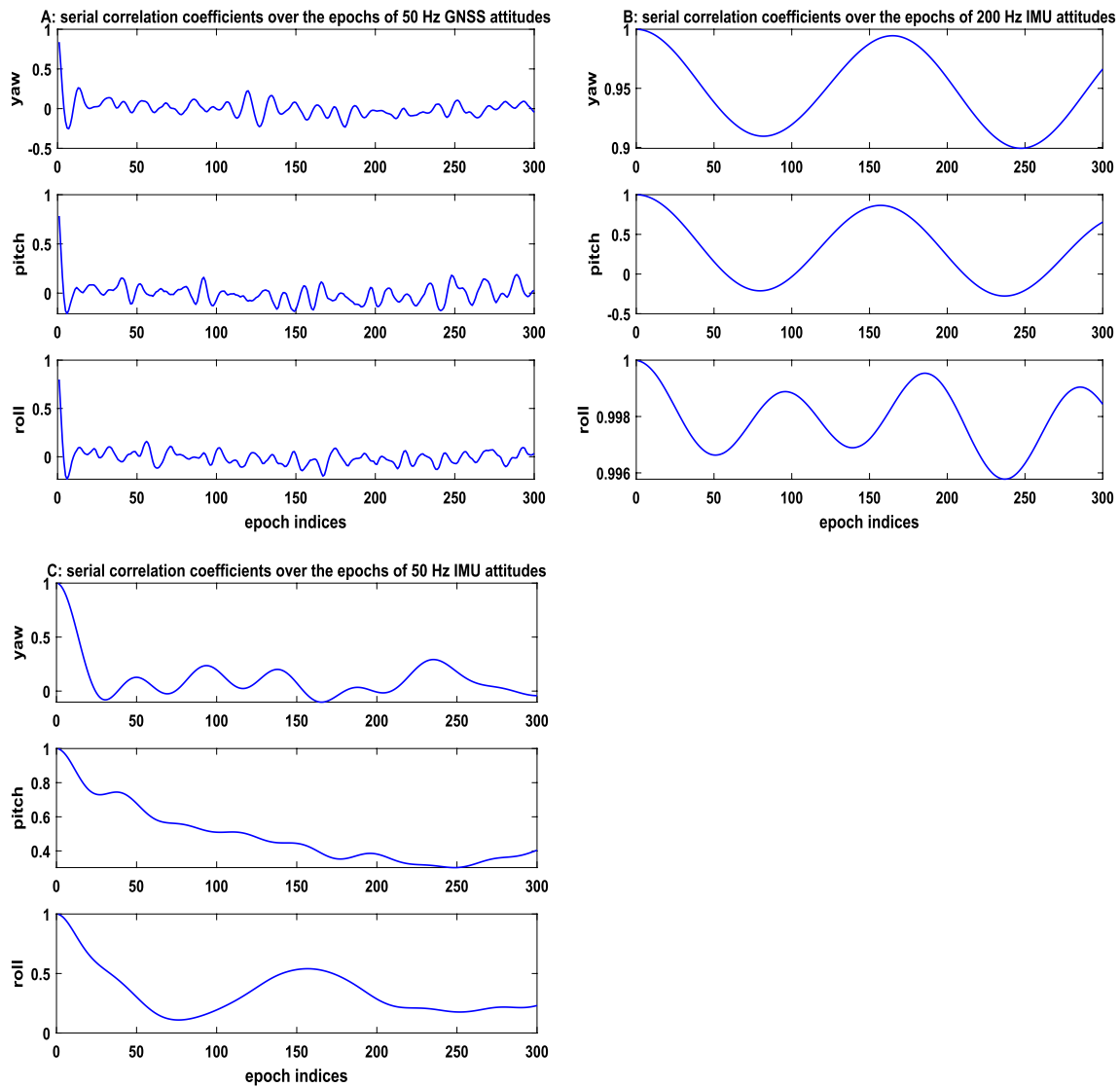


**Fig. 3** The serial correlation coefficients of high-rate GNSS and IMU attitudes over time computed with the first 18 s attitudes. Each epoch index is equivalent to 0.02 s for the 50 Hz GNSS attitudes, 0.005 s for the 200 Hz IMU attitudes, and 0.02 s for the 50 Hz IMU attitudes. Panel **A**—the serial correlation coefficients of the 50 Hz GNSS attitudes; panel **B**—the serial correlation coefficients of the 200 IMU attitudes; panel **C**—the serial correlation coefficients of the down-sampled 50 Hz IMU attitudes

to 0.66 s and then again go above 0.5 for 0.24 s after 2.82 s (or equivalently 141 epochs). The phenomena of serial correlation coefficients with both 200 Hz IMU and 50 Hz IMU static attitudes are stochastically unnormal and inconsistent, which might imply more serious problems with the IMU static attitudes. These might be related to the working principles of optical gyros but might also be related to other unknown issues of the IMU (unknown to us—the users of the IMU, at least). Because of such problems, the computed serial correlation coefficients cannot be used in our study.

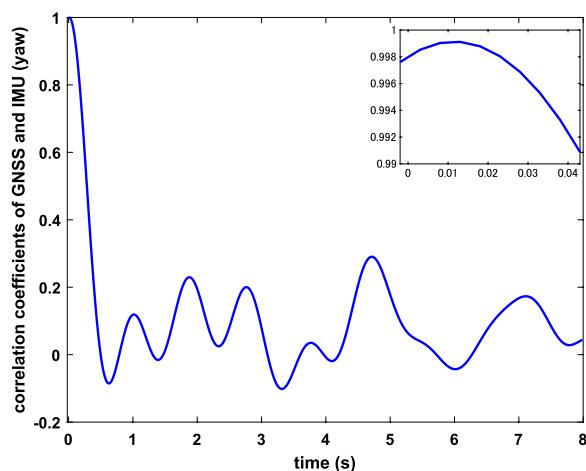
We should also like to note that although the timings of the IMU were based on its own GNSS antenna, they did not necessarily match those of GNSS exactly, as can be seen in Xu et al. (2013). In this experiment, we applied cross-correlation to both GNSS and IMU attitude time series and found a 0.015 s timing shift of the IMU NV-LINS812 ahead of GNSS. The cross-correlation coefficients of roll, pitch and yaw between GNSS and IMU attitudes are rather high, with the peak values being equal to 0.9876, 0.9967 and 0.9991, respectively. As an example, we show the cross-correlation coefficients of yaw with the maximum cross-correlation coefficient of 0.9991 in

Fig. 4, with the beginning part zoomed-in and shown on the same figure for clarity. Thus, to justify a direct comparison of GNSS and IMU and to avoid the effect of their mis-alignment, we have used the 0.015 s time shift to re-align the IMU data with those of GNSS for use in this work.

### Angular velocity and acceleration waveforms by applying difference methods to high-rate GNSS and IMU attitudes

Before presenting the regularized angular velocity and acceleration results, we apply difference methods to the combined multi-constellation 50 Hz GNSS attitudes and accordingly reconstruct the angular velocity and acceleration waveforms. Applying the error propagation law to the GNSS-differenced angular velocities and accelerations, we obtain the standard deviations of (1.9889, 1.2467, 0.5203) deg/s and (118.6779, 77.7643, 28.9059) deg/s<sup>2</sup> for the roll, pitch and yaw components, respectively. For the comparative purpose, we also compute the angular velocity and acceleration waveforms with the IMU gyro attitudes in a similar manner.

The 50 Hz GNSS- and 200 Hz IMU-derived angular velocity waveforms are shown in panels A and B of Fig. 5, respectively. By comparing the velocity results of panels A and B, in particular, the beginning parts of the velocity waveforms, we can roughly see that the amplitudes of GNSS-derived velocity waveforms are slightly larger than those derived with IMU gyro attitudes, except for the spike angular velocity of  $-35.7210$  deg/s in the roll component from IMU (compare the subplot of roll



**Fig. 4** The cross-correlation coefficients of yaw between GNSS and IMU attitudes. The first part of coefficients slightly longer than 0.04 s is amplified and shown on the upper right corner of the figure

in panel B). The ranges of amplitudes of angular velocity change between  $-28.6838$  and  $29.0015$  deg/s in roll,  $-21.3356$  and  $30.8834$  deg/s in pitch, and  $-24.3845$  and  $23.9646$  deg/s in yaw for GNSS, and between  $-35.7210$  and  $24.5817$  deg/s in roll,  $-19.1996$  and  $22.0356$  deg/s in pitch, and  $-21.6291$  and  $20.8510$  deg/s in yaw for IMU, respectively. This is likely due to the fact that the IMU gyros used in this study are more accurate to measure the attitudes than GNSS. From this point of view, we may say that the GNSS velocity results are visibly noisier. In fact, with the first 18 s of the GNSS- and IMU-based differenced velocity waveforms, we obtain the standard deviations of 1.9906, 1.2489 and 0.5203 deg/s in roll, pitch and yaw for GNSS and 0.0076, 0.0135 and 0.0089 deg/s in roll, pitch and yaw for IMU, respectively. Because there exist no true values in our experiments, it is not clear whether the IMU-computed spike velocity value of  $-35.7210$  deg/s is real or due to problems with the IMU instruments.

If we reduce the sampling rate of IMU to the same 50 Hz rate as that of GNSS, we can again compute the IMU angular velocity waveforms, which are shown in panel C of Fig. 5. Unlike the 200 Hz IMU-differenced velocity waveforms, the amplitudes of the 50 Hz IMU-derived velocity values in roll, pitch and yaw become smaller, ranging between  $-27.8525$  and  $18.4918$  deg/s,  $-17.4668$  and  $20.5527$  deg/s, and  $-20.6923$  and  $19.7760$  deg/s, respectively. Comparing the 50 Hz angular velocity results between GNSS and IMU in panels A and C, we can see that their amplitudes look roughly consistent, though GNSS results are clearly much noisier. Actually, the standard deviations of the 50 Hz IMU-derived velocity waveforms in roll, pitch and yaw are equal to 0.0035, 0.0120 and 0.0058 deg/s, as computed with the first 18 s static data, which are all smaller than the corresponding values in the case of the 200 Hz IMU-derived velocity waveforms. The reason may partially be due to the ill-posedness of the problems, because a lower sampling rate can improve reducing the standard deviations of the velocity values computed by using the difference method, though the velocities obtained stand only for the average values over a longer interval of time.

One might also like to know the differences between the 50 Hz GNSS- and 50 Hz IMU-derived angular velocity waveforms, which are plotted in panel D of Fig. 5. The difference results look far away from zero and actually are much noisier. The reason is probably due to the fact that GNSS and IMU attitude timings cannot be aligned exactly. As a result, in what follows, it may not make much sense to quantitatively compare the angular velocity and acceleration waveforms from GNSS and IMU. Instead, we can only make a qualitative

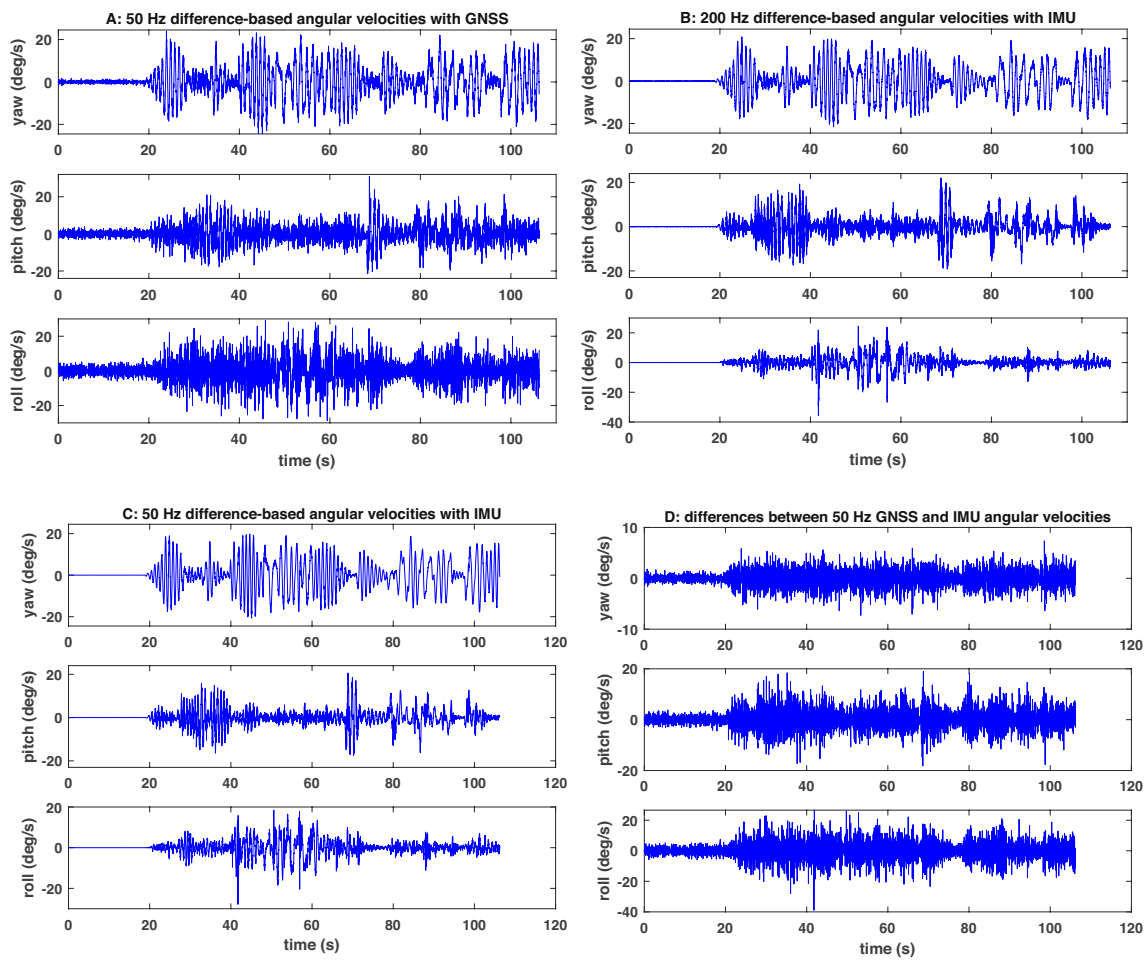


**Fig. 5** The angular velocity waveforms reconstructed by using the difference method. Also shown in this figure are the differences between the 50 Hz GNSS- and IMU-based angular velocities. Panel **A**—the 50 Hz GNSS-derived angular velocity waveforms; panel **B**—the 200 Hz IMU-derived angular velocity waveforms; panel **C**—the 50 Hz IMU-derived angular velocity waveforms aligned with GNSS; panel **D**—the differences between the 50 Hz GNSS- and IMU-derived angular velocities

comparison of angular velocity and acceleration results obtained from GNSS and IMU.

In a similar manner to computing the angular velocity waveforms from GNSS and IMU attitudes, we apply the difference method to the 50 Hz GNSS and the 200 Hz IMU attitudes and accordingly obtain their acceleration waveforms, which are shown in panels A and B of Fig. 6, respectively, ranging from  $-1841.0$  to  $1819.9$   $\text{deg/s}^2$  in roll,  $-998.3$  to  $1221.1$   $\text{deg/s}^2$  in pitch, and  $-501.3$  to  $499.2$   $\text{deg/s}^2$  in yaw for GNSS, and from  $-4099.4$  to  $3046.8$   $\text{deg/s}^2$  in roll,  $-3694.2$  to  $2616.9$   $\text{deg/s}^2$  in pitch, and  $-963.6$  to  $1321.6$   $\text{deg/s}^2$  in yaw for IMU, respectively. The signals of angular acceleration can hardly be visible in Fig. 6. Based on the first 18 s of GNSS static angular accelerations, we obtain the standard deviations of  $118.9673$ ,  $77.7303$  and  $28.9214$   $\text{deg/s}^2$  in roll, pitch and yaw, while the 18 s IMU attitudes result in very small standard deviations of  $2.4095$ ,  $2.1973$  and  $2.3892$   $\text{deg/}$

$\text{s}^2$  in the roll, pitch and yaw accelerations, respectively. Neither the standard deviations of acceleration with GNSS nor those with IMU can explain the very large fluctuations in the differenced accelerations of panels A and B. The reason may be that the noises in the GNSS and IMU attitude data have been significantly amplified, because determining angular accelerations with noisy GNSS and IMU data is ill-posed. As in the case of 50 Hz IMU angular velocities, we also compute the 50 Hz IMU angular accelerations and show the results in panel C of Fig. 6, with the standard deviations being equal to  $0.1683$ ,  $0.1754$  and  $0.1782$   $\text{deg/s}^2$  from the first 18 s static data. These values of standard deviations are extremely small in comparison of the large fluctuations of angular accelerations in panel C of Fig. 6, which might again indicate that the static attitude data of IMU may not be without problem. The differences between the 50 Hz GNSS and

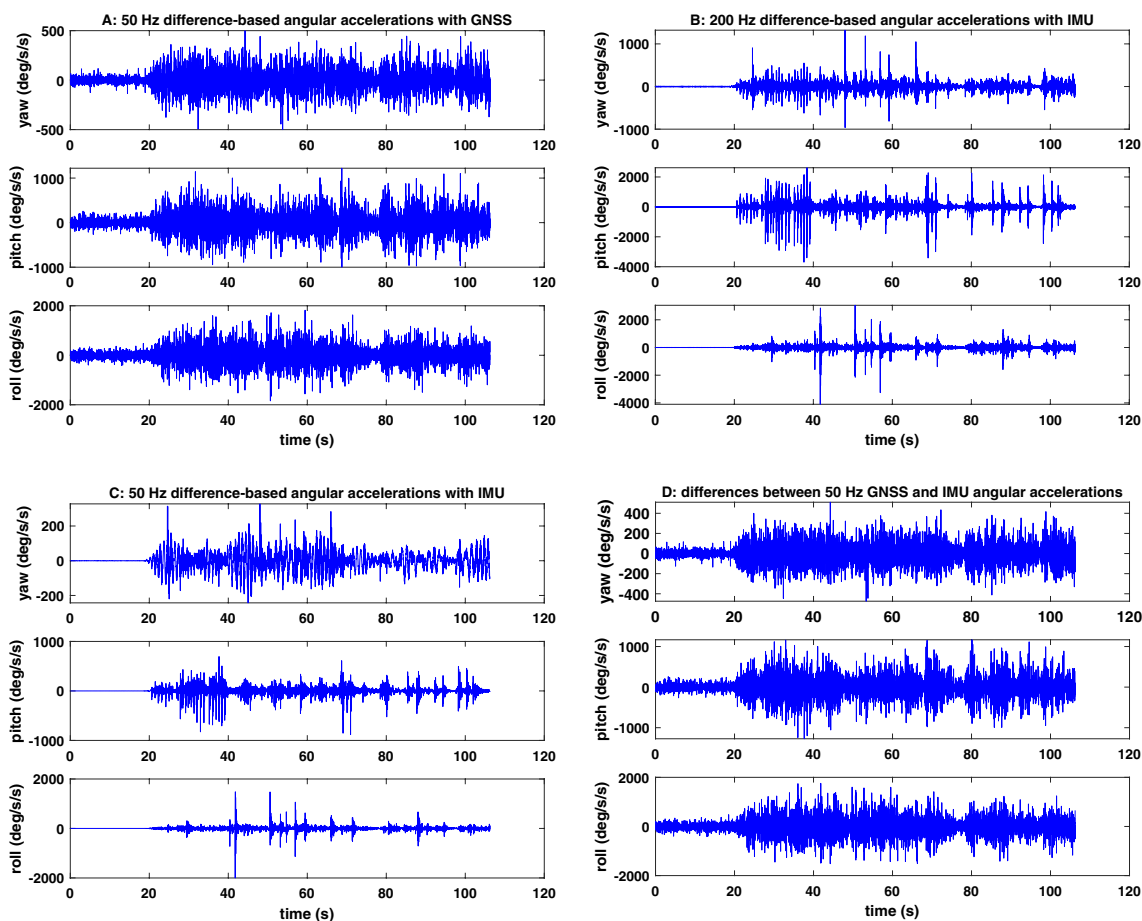


**Fig. 6** The angular acceleration waveforms reconstructed by applying the difference method to the 50 Hz GNSS and the 200 Hz IMU attitudes. Also included in this figure are the differences of the 50 Hz GNSS- and IMU-computed angular accelerations. Panel **A**—the 50 Hz GNSS-derived angular acceleration waveforms; panel **B**—the 200 Hz IMU-derived angular acceleration waveforms; panel **C**—the 50 Hz IMU-derived angular acceleration waveforms aligned with GNSS; panel **D**—the differences between the 50 Hz GNSS- and 50 Hz IMU-derived angular accelerations

50 Hz IMU angular accelerations are plotted in panel D of Fig. 6, which, once and again, confirms that the comparison of angular velocity and acceleration results between GNSS and IMU should only be qualitatively made.

### Regularized angular velocity waveforms from high-rate GNSS and IMU

Before showing the regularized solutions of angular velocity, we first show the 50 Hz angular velocities by applying the LS method to the high-rate GNSS and IMU attitudes in Fig. 7. The mean standard deviations of the LS angular velocities in roll, pitch and yaw are equal to 3.7071, 2.2336 and 1.0798 deg/s for GNSS, and 0.3302, 0.1148 and 0.1954 deg/s for IMU, respectively. When comparing the LS angular velocities in Fig. 7 with the attitude waveforms in Fig. 2, we could see that motion patterns in yaw look quite similar. However, the LS angular velocities in roll and pitch for both GNSS and IMU look very noisy. In particular, it is rather difficult to

identify the signals of velocity in the GNSS LS angular velocities in roll and pitch.

From the mathematical point of view, reconstructing angular velocity from high-rate GNSS and IMU attitudes is ill-posed. More specifically, the condition number of reconstructing angular velocities with the 50 Hz GNSS/IMU attitudes is equal to  $7.0651e+07$ . Thus, we can apply regularization to improve solutions of angular velocities, though such an improvement would depend on the ratio of  $\sigma/\Delta t$ , where  $\sigma$  and  $\Delta t$  are the accuracy of data and the time interval of velocity functions. In this and next sections, we will limit ourselves to reconstruct 50 Hz angular velocity and acceleration waveforms.

In order to apply the minimum MSE criterion for regularization, we need to know the accuracy of GNSS and IMU attitudes. For our experiments, we use the standard deviations of 0.0628, 0.0379 and 0.0183 deg in roll, pitch and yaw in the case of GNSS, and 0.0056, 0.0019 and 0.0033 deg in roll, pitch and yaw in the case of IMU,

respectively, as computed with the first 18 s static GNSS and IMU attitude data, even though experience indicates that dynamic errors can be higher. We then follow Xu et al. (2021) to first obtain a solution of an unknown function by averaging regularized solutions over a range of small regularization parameters between 0.00001 and 0.04 and then using them to determine the optimal regularization parameter for the reconstruction of angular velocity and acceleration. As a result, we obtain the optimal regularization parameters of  $1.514e-4$ ,  $0.895e-4$  and  $0.319e-4$  for roll, pitch and yaw components in the case of GNSS, and  $1.985e-5$ ,  $0.801e-5$  and  $0.973e-5$  for roll, pitch and yaw components in the case of IMU, respectively. To give the reader an impression of how the MSE values change with the regularization parameter, we use the GNSS data as an example and show the MSE plots in Fig. 8.

The regularized solutions of angular velocities for both GNSS and IMU are shown in Fig. 9. The velocity patterns for both GNSS and IMU are rather similar, though the IMU-regularized angular velocities seem to be of less noisy and larger amplitudes. Precisely speaking, the amplitudes are larger by a maximum factor of 37.55 percent in roll and a minimum factor of only about 2 percent in yaw. The regularized angular velocities from GNSS range from  $-11.5060$  to  $11.3045$  deg/s in roll,  $-11.2254$  to  $12.9545$  deg/s in pitch, and  $-18.5756$  to  $18.2544$  deg/s in yaw, respectively. They are all smaller than their counterparts in both the difference and LS solutions. More specifically, the peak regularized GNSS angular velocities in roll, pitch and yaw are smaller than those in the solutions from the difference method by a factor of 0.9

to 1.57 in roll and pitch, and by about 31 percent in yaw. The same roughly applies to the LS solutions, with a factor of 0.87–1.91 in roll and pitch, and 25 to 43 percent in yaw, respectively. In the case of regularized IMU angular velocities, these values are reduced to 26 percent to a maximum factor of 1.26 for roll and pitch, and only 12 to 14 percent in yaw when compared to those of the solutions by using the difference method. The differences between the IMU regularized and LS solutions become even smaller, with a maximum factor of 0.94 in roll and less than 21 percent for both pitch and yaw. The average MSE roots for GNSS are respectively equal to 0.7966,

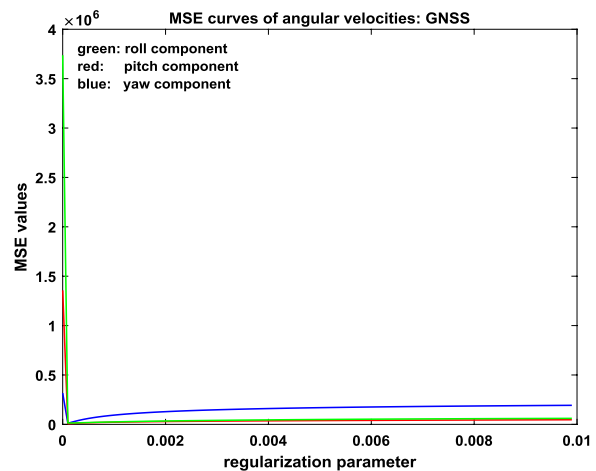


**Fig. 8** The variations of MSE values with the regularization parameter for roll, pitch and yaw components: green line—roll, red line—pitch, and blue line—yaw

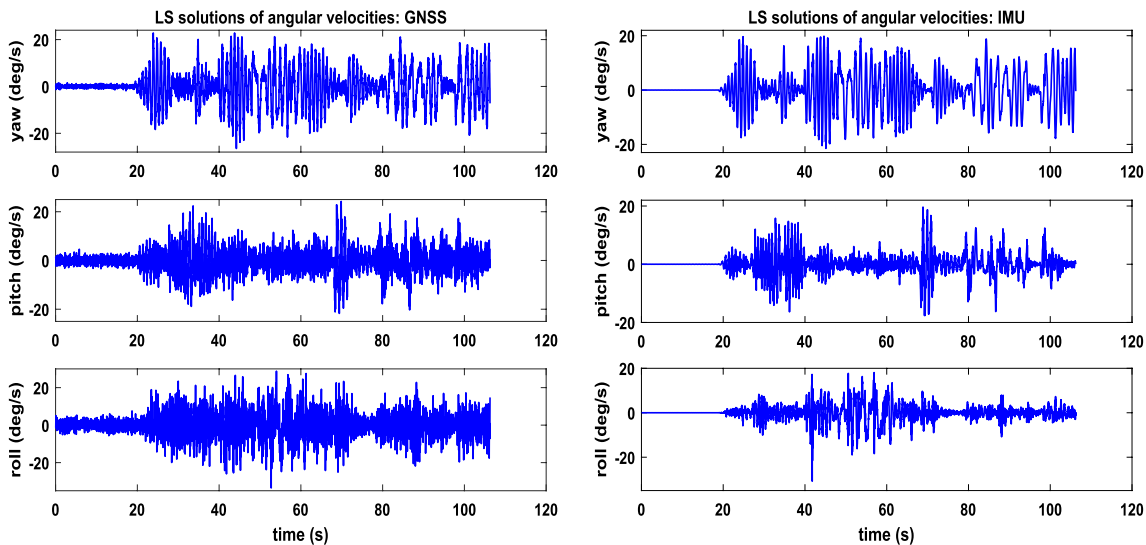


**Fig. 7** The 50 Hz solutions of angular velocities obtained by applying the LS method to the high-rate GNSS (left panel) and IMU (right panel) attitudes, respectively

0.7824 and 0.7515 deg/s for roll, pitch and yaw, which are much smaller than the corresponding average standard deviations of the LS solutions (3.7071, 2.2336 and 1.0798 deg/s), indicating that the regularized angular velocity solutions indeed improve the reconstruction of angular velocities from GNSS. To give the reader an impression on the biases of regularized angular velocities, we use the regularized angular velocity solutions to estimate their biases. The average values of the estimated biases for roll, pitch and yaw are equal to 0.0007,  $-0.0004$  and  $-0.0011$  deg/s in the case of GNSS, and 0.0001,  $-0.0001$  and  $-0.0005$  deg/s in the case of IMU, respectively. Similarly, the median values of the absolute estimated biases of regularized angular velocities for roll, pitch and yaw are equal to 0.3595, 0.3197 and 0.3537 deg/s in the case of GNSS, and 0.1404, 0.0893 and 0.1176 deg/s in the case of IMU, respectively.

### Regularized angular acceleration waveforms from high-rate GNSS and IMU

Given the 50 Hz GNSS and IMU attitudes, we apply the eigenvalue function eig of Matlab R2021a and determine the condition number of the normal matrix  $A^T A$  for the discretized linear observation equation (8) in association of angular acceleration, which is found to be almost as large as  $1.0e+20$ . With such an extremely large condition number, any noise in the measured data would be roughly amplified by a factor of  $1.0e+10$ . Actually, the computation of the exact condition number is difficult and likely not very reliable for these examples with Matlab R2021a. As a result, no physically meaningful results of

angular accelerations can be expected, if the LS method is applied. As in the case of the regularized solutions of angular velocity, we first show the 50 Hz LS angular accelerations with both the 50 Hz high-rate GNSS and 50 Hz IMU attitudes in Fig. 10. It is clear from Fig. 10 that the LS solutions of angular accelerations are too noisy to be physically useful, as theoretically expected. Thus, we will not go into any details of these solutions.

We now apply regularization under the criterion of minimum MSE to reconstruct angular acceleration waveforms with the average regularized solution obtained over a small range of regularization parameters between 0.0001 and 0.002. The optimal regularization parameters are equal to  $1.051e-05$  in roll,  $0.298e-05$  in pitch and  $0.177e-05$  in yaw for GNSS, and  $8.797e-07$  in roll,  $2.204e-07$  in pitch and  $3.151e-07$  in yaw for IMU, respectively. The optimal regularization parameters for IMU are much smaller than those for GNSS by a factor of 10.95 in roll, 12.52 in pitch and 4.62 in yaw, respectively. The reason is likely due to the fact that the IMU attitudes are much more precise than the GNSS attitudes. Given an inverse ill-posed problem, a small variance tends to result in a smaller regularization parameter to arrive at the minimum MSE.

The regularized angular acceleration solutions with both high-rate GNSS and IMU attitudes are shown in Fig. 11. A quick comparison of panels A and B of Fig. 6, Fig. 10 and Fig. 11 can immediately conclude that the regularized angular accelerations are only an extremely small fraction of those computed either by using the difference method or the LS method. More precisely,

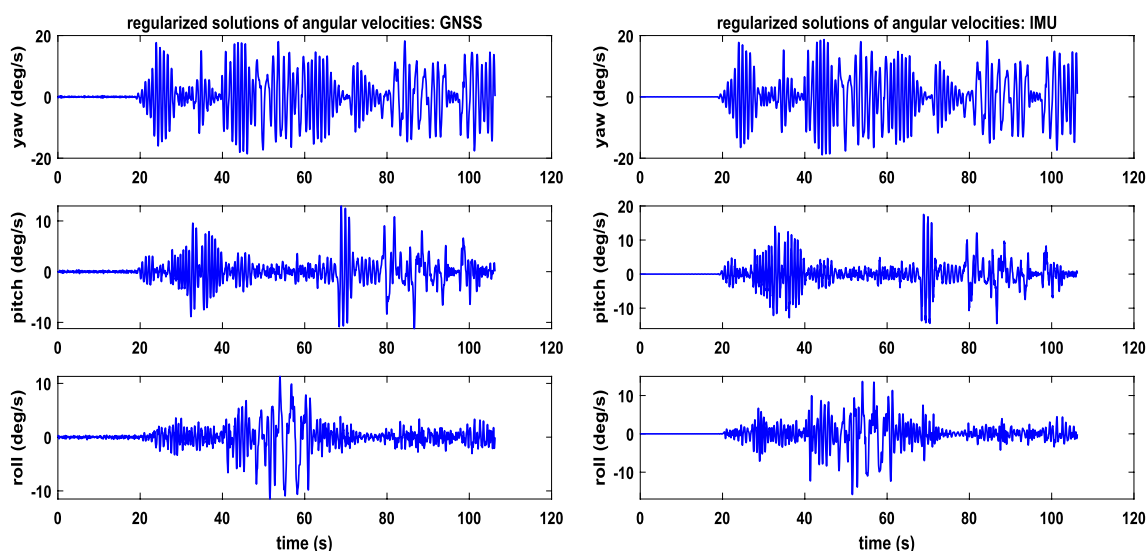


**Fig. 9** The regularized angular velocity solutions from the combined multi-constellation 50 Hz GNSS and IMU raw attitudes, respectively. Left panel: the regularized angular velocity solutions with GNSS attitudes; right panel: the regularized angular velocity solutions with the gyro attitudes of NV-LINS812

the peak regularized angular accelerations are smaller than those with the difference method by a maximum factor of 8662.53 in the case of GNSS and 2819.85 in the case of IMU, respectively.

In fact, the mean MSE roots of regularized angular accelerations with IMU attitudes are estimated to be equal to 0.1886, 0.3096 and 0.4366  $\text{deg/s}^2$  in roll, pitch and yaw, respectively, indicating that the regularized solutions of angular acceleration are reasonable. As in the case of regularized angular velocities, we also use the regularized angular acceleration solutions to estimate their biases. On average, the biases for roll, pitch and yaw are equal to 0.00004,  $-0.00068$  and  $-0.00031$   $\text{deg/s}^2$  in the case of GNSS and, 0.00016, 0.00007 and  $-0.00128$   $\text{deg/s}^2$  in the case of IMU, respectively. The median values of the absolute estimated biases of regularized angular acceleration solutions for roll, pitch and yaw are equal to 0.00573, 0.01716 and 0.03209  $\text{deg/s}^2$  in the case of GNSS and, 0.01270, 0.05180 and 0.10824  $\text{deg/s}^2$  in the case of IMU, respectively. It is a bit surprised to see that these mean and median values are larger in the case of IMU than GNSS, even though the regularization parameters are smaller in the case of IMU. The reason is likely due to the fact that the regularized angular accelerations are larger in the case of IMU. The examples may indicate that one should interpret the computed bias values with care, since they are estimated with uncertainty.

It is clear from Fig. 11 that the regularized angular accelerations with GNSS are smaller than those with IMU. Since the IMU attitudes are more accurate than the high-rate GNSS attitudes, the regularized IMU angular

accelerations should be more accurate. The regularized angular accelerations range from  $-0.2125$  to  $0.2163$   $\text{deg/s}^2$  in roll,  $-0.5921$  to  $0.7464$   $\text{deg/s}^2$  in pitch, and  $-0.6629$  to  $0.6503$   $\text{deg/s}^2$  in yaw for GNSS, and from  $-1.5306$  to  $1.0801$   $\text{deg/s}^2$  in roll,  $-2.1916$  to  $3.0086$   $\text{deg/s}^2$  in pitch, and  $-2.9581$  to  $1.9685$   $\text{deg/s}^2$  for IMU, respectively. The peak regularized angular accelerations with IMU are larger than those with GNSS by a factor of 6.20 in roll, 3.03 in pitch and 3.46 in yaw, respectively. The reason is that the noise levels of GNSS attitudes are much higher than those of IMU attitudes. As a result, an effective suppression of GNSS noise amplification for regularized angular accelerations requires a larger regularization parameter, which, in turn, would shrink the angular accelerations.

To further validate this explanation, we use the IMU-based optimal regularization parameters to reconstruct the angular accelerations from high-rate GNSS attitudes. In a similar manner, we can also reconstruct the IMU angular accelerations with the GNSS-based optimal regularization parameters. The results of cross-comparison between GNSS and IMU are shown in Fig. 12. The regularized IMU angular accelerations are basically identical to the regularized GNSS angular accelerations with the optimal IMU-based regularization parameters, as can be seen by comparing the acceleration plots in the right panel of Fig. 11 with those in the left panel of Fig. 12. The same is true about the regularized GNSS angular accelerations in the left panel of Fig. 11 and the regularized IMU angular accelerations with the optimal GNSS-based regularization parameters in the right panel of Fig. 12. All these results clearly indicate that more

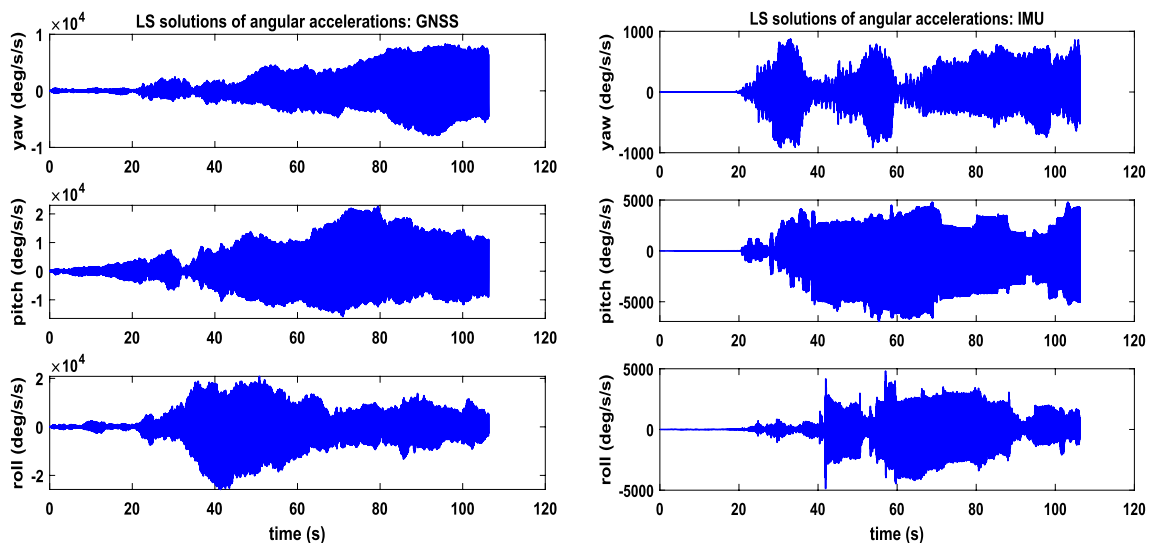


**Fig. 10** The 50 Hz solutions of angular accelerations obtained by applying the LS method to the high-rate GNSS (left panel) and IMU (right panel) attitudes, respectively

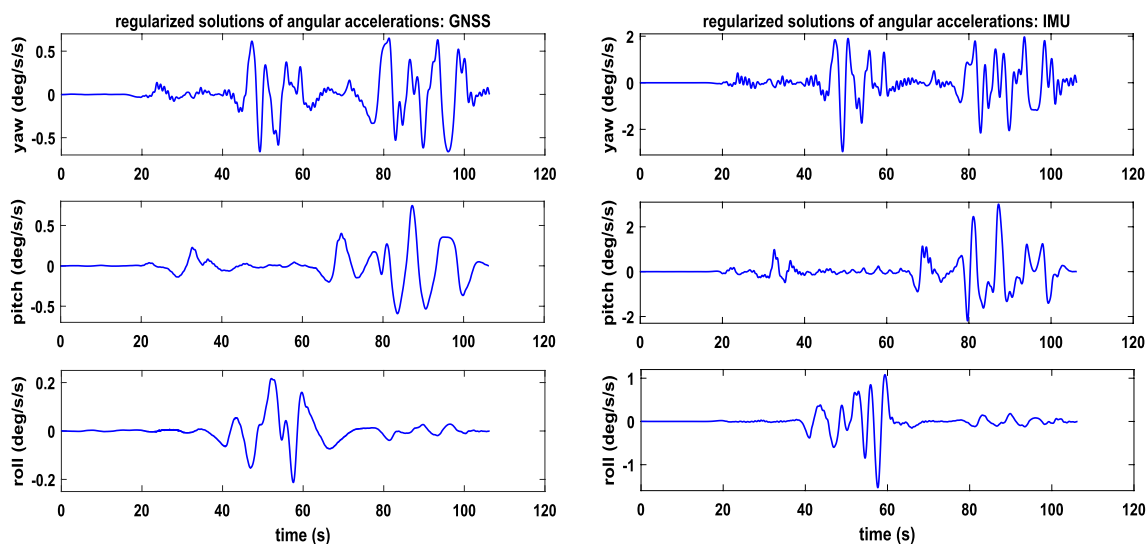


**Fig. 11** The regularized angular acceleration solutions from the combined multi-constellation 50 Hz GNSS and IMU raw attitudes, respectively. Left panel: the regularized angular acceleration solutions with GNSS attitudes; right panel: the regularized angular acceleration solutions with the gyro attitudes of NV-LINS812

accurate measured data results in more accurate regularized solutions, as already consistently reported in Xu (2023). They apparently imply that the accuracy estimate of GNSS attitudes with the static data seems appropriate to reconstruct angular accelerations from GNSS. A likely larger dynamical GNSS attitude error (if so used) would be expected to further shrink regularized angular accelerations in the case of GNSS. Finally, we may like to note that unless the timings of GNSS and IMU are exactly aligned with each other, such a timing mis-alignment can significantly affect a scientifically fair comparison of the reconstructed angular accelerations with GNSS and IMU, which may hardly be possible. At the very least, such a comparison must be done with great care with the timing mis-alignment in mind.

## Conclusions

Attitude and pose information has been becoming increasingly important in many areas of science and engineering. Attitudes of rigid objects and/or poses of human beings can either be directly measured precisely with gyro instruments or indirectly with GNSS and cameras. Although angular velocity and acceleration are also important physical quantities with important industrial applications, they are generally computed from attitudes, which has been shown in this paper to be inverse ill-posed problems, as in the case of determining translational velocity and acceleration in Xu et al. (2021) and Xu (2023). As a result, noise in raw measurements and/or attitudes can be extremely magnified, depending on

accuracy of measurements and the extent of ill-posedness of such problems.

We have proposed the ideas and concept of GNSS gyroscopes and paid particular attention to angular velocity and acceleration as its two key components. We have reformulated the differential equations of angular velocity and acceleration as the equivalent integral equations of the first kind, discretized them and applied regularization to accurately reconstruct angular velocity and acceleration. Experiments carried out in 2014 scientifically fit perfectly the purpose of demonstrating the concept of GNSS gyroscopes and have been satisfactorily used to validate all our ideas proposed in this work, even though they were originally designed mainly to determine high-rate GNSS attitudes, as reported in Xu et al. (2019) and Shu et al. (2022). More interestingly, the 2014 experiments were involved with both GNSS and IMU instruments. Thus, we can fully use them for the purpose of comparison and for illustrating some important aspects of regularized reconstruction of angular velocity and acceleration.

The difference and LS methods have been applied to compute angular velocity and acceleration. Reconstruction of angular velocity is shown to be moderately ill-posed. If attitudes are sufficiently precise, the computed angular velocities could be satisfactory with both GNSS and IMU attitudes, depending on what resolution would be required. With the increase of resolutions, the condition number can become very large such that computed angular velocities with either of the methods can become very unreliable. Because reconstruction of angular

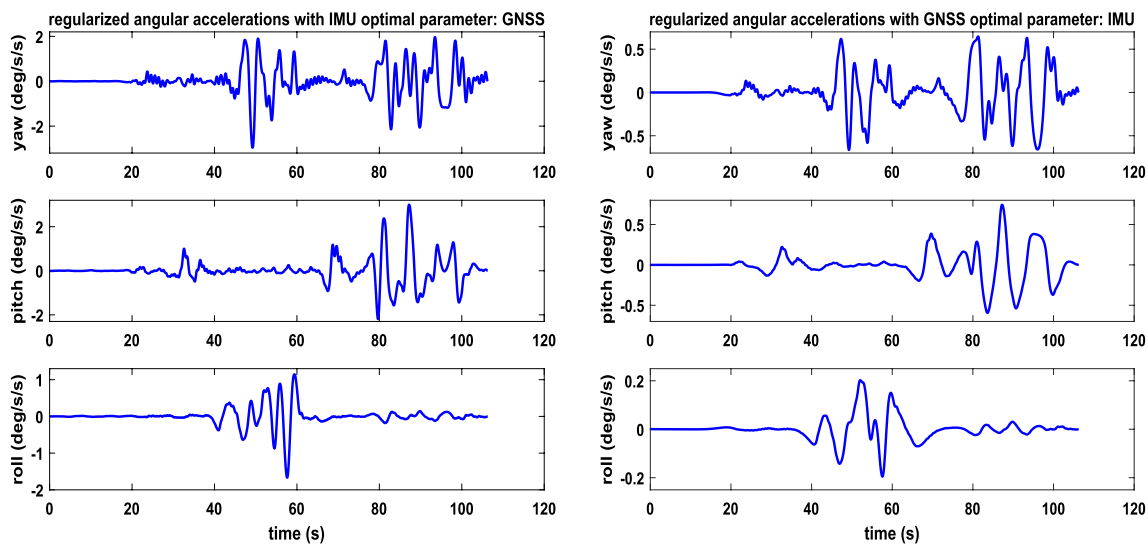


**Fig. 12** The regularized angular acceleration solutions obtained from the high-rate GNSS attitudes but with the IMU-based optimal regularization parameters and from the raw IMU attitudes but with the GNSS-based optimal regularization parameters, respectively. Left panel: the regularized GNSS angular acceleration waveforms with the optimal regularization parameters determined on the basis of the IMU attitudes; right panel: the regularized IMU angular acceleration waveforms with the optimal regularization parameters determined on the basis of the high-rate GNSS attitudes

acceleration is severely ill-posed, we have shown with both high-rate GNSS and IMU attitudes that neither the difference method nor the LS method can produce any physically meaningful solutions to angular accelerations. The signals of angular accelerations have been completely drowned into the noises of such solutions.

We have applied regularization to reconstruct angular velocity and acceleration from high-rate GNSS and IMU attitudes. Even with a moderate ill-posedness of angular velocity problems, the regularized reconstruction of angular velocities has been shown to be significantly more accurate than that by using either the difference or LS method. On the other hand, since IMU attitudes are more precise, the corresponding regularized angular velocity solutions are shown to be more accurate as well. Regularization has been successfully applied to accurately reconstruct angular accelerations from high-rate GNSS and IMU attitudes. Unlike the solutions of angular accelerations with either the difference or LS method, the angular acceleration signals can be clearly visible in the regularized solutions, which are only a very small fraction of those obtained from the difference and LS methods. The regularization results of angular accelerations have also shown that less accurate data would demand a larger regularization parameter to effectively suppress or control the magnification of noise. More accurate data can significantly improve the reconstruction of angular acceleration signals, as cross-validated by applying the IMU-based optimal regularization parameters to

high-rate GNSS attitudes and vice versa, and as can be seen in Xu (2023). Finally, we may like to note that static data from optical IMU gyros should be used and evaluated with care. Combining GNSS and IMU attitudes to reconstruct angular velocities and accelerations can be a topic for future work, in particular, if only one GNSS baseline is available. Further work on regularization is also highly expected.

#### Acknowledgements

The authors thank the reviewers for their constructive comments, which help further improve the manuscript.

#### Author contributions

PX conceived all the ideas and developed the methods for this research. PX and Yun Shi designed the numerical experiments. Yun Shi and PX prepared and wrote the computational codes and performed the numerical experiments. Yuanming Shu collected GNSS and IMU data and computed the GNSS attitudes for this work. PX, XM and Yun Shi discussed the computation results. PX and Yun Shi wrote the manuscript. All the authors reviewed the manuscript.

#### Funding

This work is partially supported by the National Natural Science Foundation of China under projects Nos. 42174045 and 41874012 awarded to Yun Shi.

#### Data availability

The data sets used and/or analysed during the current study are available from the corresponding author on reasonable request.

#### Declarations

#### Competing interests

Peiliang Xu and Xiaolin Meng are the editorial board members of *Satellite Navigation* but were not involved in the review and decision processes to publish this article. The authors declare that they have no competing interests.

**Author details**

<sup>1</sup>School of Geomatics, Xi'an University of Science and Technology, Xi'an 710054, People's Republic of China. <sup>2</sup>Disaster Prevention Research Institute, Kyoto University, Uji, Kyoto 611-0011, Japan. <sup>3</sup>College of Marine Geosciences, Ocean University of China, Qingdao, People's Republic of China. <sup>4</sup>School of Instrument Science and Engineering, Southeast University, Nanjing 210096, People's Republic of China.

Received: 13 November 2023 Accepted: 21 December 2023

Published online: 19 March 2024

**References**

- Akaike, H. (1980). Likelihood and the Bayes procedure. In J. M. Bernardo, M. H. de Groot, D. V. Lindley, & A. F. M. Smith (Eds.), *Bayesian statistics* (pp. 1–13). University Press.
- Ardalan, A. A., & Rezvani, M. (2015). An iterative method for attitude determination based on misaligned GNSS baselines. *IEEE Transactions on Aerospace and Electronic Systems*, *51*, 97–106.
- Armenise, M. N., Ciminelli, C., Dell'Olio, F., & Passaro, V. M. N. (2010). *Advances in gyroscope technologies*. Springer.
- Bashnick, C., & Ulrich, S. (2023). Fast model predictive control for spacecraft rendezvous and docking with obstacle avoidance. *Journal of Guidance, Control, and Dynamics*, *46*, 998–1007.
- Bennett, G. G. (1970). An historical review of the development of the gyroscope. *Australian Surveyor*, *23*, 244–252. <https://doi.org/10.1080/00050326.1970.10440242>
- Bertrand, M. J. (1857). Note on Foucault's gyroscope. *The London, Edinburgh, and Dublin Philosophical Magazine and Journal of Science*, *13*, 31–33.
- Black, H.D. (1964). A passive system for determining the attitude of a satellite. *AIAA Journal*, *2*, 1350–1351.
- Cannon, M. E., & Sun, H. (1996). Experimental assessment of a non-dedicated GPS receiver system for airborne attitude determination. *ISPRS Journal of Photogrammetry and Remote Sensing*, *51*, 99–108.
- Chindamo, D., Lenzo, B., & Gadola, M. (2018). On the vehicle sideslip angle estimation: A literature review of methods, models, and innovations. *Applied Sciences*, *8*, 355.
- Cohen, C. E. (1992). *Attitude determination using GPS: Development of an all solid-state guidance, navigation, and control sensor for air and space vehicles based on the global positioning system*. PhD Thesis, Stanford University
- Cohen, C. E., Parkinson, B. W., & McNally, B. D. (1993). Flight tests of attitude determination using GPS compared against an inertial navigation unit. In *Proceedings of ION NTM 1993, San Francisco, CA, 1993*, pp. 579–587.
- Cordeiro, F. J. B. (1913). *The gyroscope: Theory and applications*. Spon & Chamberlain.
- Crassidis, J. L., Markley, F. L., & Cheng, Y. (2007). Survey of nonlinear attitude estimation methods. *Journal of Guidance, Control, and Dynamics*, *30*, 12–28.
- De Vito, L., Mazzilli, G., Riccio, M., & Sementa, C. (2016). Improving the orientation estimation in a packet loss-affected wireless sensor network for tracking human motion. In *Proceedings of the 21th IMEKO TC4 International Symposium Understanding the World through Electrical Electronics Measurement & 19th International Work. ADC Model. Testing, Budapest, Hungary, September 7–9, 2016*, pp. 184–189.
- De Vito, L., Postolache, O., & Rapuano, S. (2014). Measurements and sensors for motion tracking in motor rehabilitation. *IEEE Instrumentation & Measurement Magazine*, *17*, 30–38.
- Eling, C., Klingbeil, L., & Kuhlmann, H. (2015). Real-time single-frequency GPS/MEMS-IMU attitude determination of lightweight UAVs. *Sensors*, *15*, 26212–35.
- Ellis, J., & Creswell, G. (1979). Interferometric attitude determination with the Global Positioning System. *Journal of Guidance and Control*, *2*, 522–527.
- Endo, Y., Yagi, K., Mori, Y., Takei, T., & Mochiyama, H. (2023). Tele-Snap: a joint impedance estimation system using snap motor and openPose for remote rehabilitation diagnosis. *Advanced Robotics*, *37*, 528–539. <https://doi.org/10.1080/01691864.2023.2197968>
- Evans, A. G. (1986). Roll, pitch, and yaw determination using a global positioning system receiver and an antenna periodically moving in a plane. *Marine Geodesy*, *10*, 43–52.
- Fujii, Y., Fukumi, M., Ito, S., & Ito, M. (2020). Detection of dangerous objects by pan-tilt camera. In *Proceedings of the international symposium intelligent signal processing communication system (ISPACS)*, Taipei, Taiwan province of China. 03–06 December 2019. <https://doi.org/10.1109/ISPACS48206.2019.8986233>
- Fujiwara, K., & Yokomitsu, K. (2021). Video-based tracking approach for nonverbal synchrony: A comparison of motion energy analysis and OpenPose. *Behavior Research Methods*, *53*, 2700–2711.
- Golub, G. M., Heath, M., & Wahba, G. (1979). Generalized cross-validation as a method for choosing a good ridge parameter. *Technometrics*, *21*, 215–223.
- Hashim, H. A., & Lewis, F. L. (2021). Nonlinear stochastic estimators on the special Euclidean group SE(3) using uncertain IMU and vision measurements. *IEEE Transactions on Systems, Man, and Cybernetics: Systems*, *51*, 7587–7600.
- Hoerl, A. E., & Kennard, R. W. (1970). Ridge regression: Biased estimation for nonorthogonal problems. *Technometrics*, *12*, 55–67.
- Hofmann-Wellenhof, B., Lichtenegger, H., & Collins, J. (1992). *GPS theory and practice*. Springer.
- Horn, B., Hilden, H. M., & Negahdripour, S. (1988). Closed-form solution of absolute orientation using orthonormal matrices. *Journal of the Optical Society of America. A, Optics and image science*, *5*, 1127–1135.
- Igel, H., Cochard, A., Wassermann, J., Flaws, A., Schreiber, U., Velikoseltsev, A., & Dinh, N. P. (2007). Broad-band observations of earthquake-induced rotational ground motions. *Geophysical Journal International*, *168*, 182–196.
- Islam, M. M., Lam, A., Fukuda, H., Kobayashi, Y., & Kuno, Y. (2019). An intelligent shopping support robot: understanding shopping behavior from 2D skeleton data using GRU network. *Robomech Journal*, *6*, 18.
- Jeong, T., & Ha, I. (2023). OpenPose based smoking gesture recognition system using artificial neural network. *Tehnicki Glasnik*, *17*, 251–259.
- Keat, J. E. (1977). *Analysis of least-squares attitude determination routine DOAOP*. Technical Report CSC/TM-77/6034. Computer Sciences Corporation.
- Kinsey, J. C., Eustice, M. R., & Whitcomb, L. L. (2006). A survey of underwater vehicle navigation: Recent advances and new challenges. In *Proceedings of the IFAC conference Manoeuvring control marine craft*, vol. 88, pp. 1–12.
- Lachapelle, G., Cannon, M., Lu, G., & Loncarevic, B. (1996). Shipborne GPS attitude determination during MMST-93. *IEEE Journal of Oceanic Engineering*, *21*, 100–104.
- Lee, W. H. K., Celebi, M., Todorovska, M. I., & Igel, H. (2009). Introduction to the special issue on rotational seismology and engineering applications. *Bulletin of the Seismological Society of America*, *99*, 945–957.
- Leung, K. T., Whidborne, J. F., Purdy, D., & Dunoyer, A. (2011). A review of ground vehicle dynamic state estimations utilising GPS/INS. *Vehicle System Dynamics*, *49*, 29–58.
- Lonseth, A.T. (1977) Sources and applications of integral equations. *SIAM Review*, *19*, 241–278.
- Linnainmaa, S., Harwood, D., & Davis, L. S. (1988). Pose determination of a three-dimensional object using triangle pairs. *IEEE Transactions on Pattern Analysis and Machine Intelligence*, *10*, 634–647.
- Lubansky, A.S., Yeow, Y.L., Leong, Y.-K., Wickramasinghe, S.R. & Han, B. (2006). A general method of computing the derivative of experimental data. *AIChE Journal*, *52*, 323–332.
- Lu, G. (1995) *Development of a GPS multi-antenna: System for attitude determination*. PhD Thesis, UCGE Reports No.20073. Department of Geomatics Engineering, The University of Calgary, Calgary.
- Lu, G., Cannon, M., Lachapelle, G., & Kielland, P. (1994). Attitude determination using dedicated and nondedicated multi-antenna GPS sensors. *IEEE Transactions on Aerospace and Electronic Systems*, *30*, 1053–1058.
- Markley, F.L. & Mortari, D. (2000). Quaternion attitude estimation using vector observations. *Journal of Astronautical Science*, *48*, 359–380.
- Markley, F.L. (2002). Fast quaternion attitude estimation from two vector measurements. *Journal of Guidance, Control and Dynamics*, *25*, 411–414.
- Nose, T., Kitamura, K., Oono, M., Nishida, Y., & Ohkura, M. (2020). Data-driven child behavior prediction system based on posture database for fall accident prevention in a daily living space. *Journal of Ambient Intelligence and Humanized Computing*, *11*, 5845–5855.
- Passaro, V. M. N., Cuccovillo, A., Vaiani, L., De Carlo, M., & Campanella, C. E. (2017). Gyroscope technology and applications: A review in the industrial perspective. *Sensors*, *17*, 2284.
- Phillips, D. L. (1962). A technique for the numerical solution to certain integral equations of the first kind. *Journal of the ACM*, *9*, 84–97.

- Reid, H. F. (1910). *The California earthquake of April 18, 1906 the mechanics of the earthquake, report of the state earthquake investigation commission* (Vol. 2). Carnegie Institution of Washington.
- Richards, J. (1999). The measurement of human motion: A comparison of commercially available systems. *Human Movement Science*, 18, 589–602.
- Royer, E., Lhuillier, M., Dhome, M., & Lavest, J. (2007). Monocular vision for mobile robot localization and autonomous navigation. *International Journal of Computer Vision*, 74, 237–260.
- Schönemann, P. H. (1964) *A solution of the orthogonal procrustes problem with applications to orthogonal and oblique rotation*. Ph.D. dissertation, University of Illinois.
- Segal, S., Carmi, A., & Gurfı, P. (2014). Stereovision-based estimation of relative dynamics between noncooperative satellites: Theory and experiments. *IEEE Transactions on Control Systems Technology*, 22, 568–584.
- Shuster, M.D. & Oh, S.D. (1981). Three-axis attitude determination from vector observations. *Journal of Guidance Control*, 4, 70–77.
- Shu, Y. M., Xu, P. L., Niu, X. J., Chen, Q., Qiao, L., & Liu, J. N. (2022). High-rate attitude determination of moving vehicles with GNSS: GPS, BDS, GLO-NASS and Galileo. *IEEE Transactions on Instrumentation and Measurement*. <https://doi.org/10.1109/TIM.2022.3168896>
- Sommeria, J. (2017). Foucault and the rotation of the Earth. *Comptes Rendus Physique*, 18, 520–525.
- Takeo, M. (2009). Rotational motions observed during an earthquake swarm in April 1998 offshore Ito, Japan. *Bulletin of the Seismological Society of America*, 99, 1457–1467.
- Tarantola, A. (1987). *Inverse problem theory: Methods for data fitting and model parameter estimation*. Elsevier.
- Tikhonov, A. N., & Arsenin, V. Y. (1977). *Solutions of ill-posed problems*. John Wiley & Sons.
- Tobin, W. (2023). The life and science of Léon Foucault as a muse. In S. Gullberg & P. Robertson (Eds.), *Essays on astronomical history and heritage, historical & cultural astronomy* (pp. 113–141). Springer. [https://doi.org/10.1007/978-3-031-29493-8\\_6](https://doi.org/10.1007/978-3-031-29493-8_6)
- Van Graas, F., & Braasch, M. (1991). GPS interferometric attitude and heading determination: Initial flight test results. *Navigation*, 38, 297–316.
- Wahba, G. (1965). A least squares estimate of spacecraft attitude. *SIAM Review*, 7, 409.
- Xia, X., Hashemi, E., Xiong, L., & Khajepour, A. (2023). Autonomous vehicle kinematics and dynamics synthesis for sideslip angle estimation based on consensus Kalman filter. *IEEE Transactions on Control Systems Technology*, 31, 179–192.
- Xu, P. L. (2023). *The concept of computerized accelerometers*. <https://doi.org/10.21203/rs.3.rs-2575585/v1>
- Xu, P. L. (1992). Determination of surface gravity anomalies using gradiometric observables. *Geophysical Journal International*, 110, 321–332.
- Xu, P. L. (1998). Truncated SVD methods for linear discrete ill-posed problems. *Geophysical Journal International*, 135, 505–514.
- Xu, P. L. (2009). Iterative generalized cross-validation for fusing heteroscedastic data of inverse ill-posed problems. *Geophysical Journal International*, 179, 182–200. <https://doi.org/10.1111/j.1365-246X.2009.04280.x>
- Xu, P. L. (2021). A new look at Akaike's Bayesian information criterion for inverse ill-posed problems. *Journal of the Franklin Institute*, 358, 4077–4102. <https://doi.org/10.1016/j.jfranklin.2021.03.003>
- Xu, P. L., Du, F., Shu, Y., Zhang, H. P., & Shi, Y. (2021). Regularized reconstruction of peak ground velocity and acceleration from very high-rate GNSS precise point positioning with applications to the 2013 Lushan Mw6.6 earthquake. *Journal of Geodesy*. <https://doi.org/10.1007/s00190-020-01449-6>
- Xu, P. L., Shi, C., Fang, R. X., Liu, J. N., Niu, X. J., Zhang, Q., & Yanagidani, T. (2013). High-rate precise point positioning (PPP) to measure seismic wave motions: An experimental comparison of GPS PPP with inertial measurement units. *Journal of Geodesy*, 87, 361–372. <https://doi.org/10.1007/s00190-012-0606-z>
- Xu, P. L., Shu, Y., Niu, X., Liu, J. N., Yao, W., & Chen, Q. (2019). High-rate multi-GNSS attitude determination: experiments, comparisons with inertial measurement units and applications of GNSS rotational seismology to the 2011 Tohoku Mw9.0 earthquake. *Measurement Science and Technology*, 30, 024003. <https://doi.org/10.1088/1361-6501/aaf987>
- Yazdi, N., Ayazi, F., & Najafi, K. (1998). Micromachined inertial sensors. *Proceedings of the IEEE*, 86, 1640–1659.
- Zhao, X., & Zhang, S. (2022). Image-feature-based integrated path planning and control for spacecraft rendezvous operations. *Journal of Guidance, Control, and Dynamics*, 45, 830–845.

## Publisher's Note

Springer Nature remains neutral with regard to jurisdictional claims in published maps and institutional affiliations.